Axisymmetric Analysis and Design of Ducted Rotors

Mark Drela [1]   **Harold Youngren** [2]

Draft 30 Jan 05

Summary

This report describes the analytical formulation used for the design and analysis of a ducted propulsor with single or multiple blade rows. It is based on a lifting-line representation of the rotor blade together with an axisymmetric panel representation of the duct and centerbody. The induced velocities associateed with blade-row loading are represented by vortex sheets shed into the flowfield. Blade element models are used for blade row sections using two-dimensional lift, moment and profile drag characteristics to account for loading and viscous losses.

The modeling fidelity of the present approach lies between classical vortex/blade-element methods of Betz [1] and Glauert [2], and a general 3-D vortex-lattice or panel method. Even the general 3-D formulations would have to make the same time-averaging assumptions for the unsteady counter-rotating flow as the present method, and hence would not be more sophisticated or more accurate in this regard. The chief advantage of the present method is that it is extremely fast computationally and is has simple inputs, making it ideal for interactive design work.

The formulation described here derives in part from the existing propeller design/analysis code XROTOR, which combines classical propeller theory with some simple models for the effects of a duct and centerbody. XROTOR's simple duct treatment ignores the details of the duct velocity field and the effect of losses in the duct flowpath, both of which have a strong influence on flow conditions on the rotor. In contrast, the present formulation includes a more detailed treatment of the following effects.

- Reformulation to allow arbitrarily large induced velocities relative to the freestream velocity. This is necessary to treat the hovering case where the "freestream" velocity vanishes.

- Incorporation of a shrouded tip and center body into the self-induced velocity formulation.

- Inclusion of loss effects and non-uniform loading effects in the duct flowfield calculation.

Nomenclature

r, θ, x	cylindrical coordinates
ξ, η	grid coordinates (in grid section)
ξ, η, ζ	helical coordinates (in blade geometry section)
m	meridional coordinate: $\quad dm^2 = dx^2 + dr^2$
m'	stretched meridional coordinate: $\quad dm' = dm/r$
ρ	density
p	static pressure
p_o	total pressure
H	total enthalpy
s	entropy
S	kinematic entropy ($\equiv s\, p/\rho$)
V_∞	freestream speed along rotor axis

---

[1]MIT Aero & Astro Dept.

[2]Aerocraft, Inc.

$\vec{v}$	self-induced velocity
$\vec{u}$	externally-induced velocity
$\vec{V}$	total velocity relative to duct
$\vec{W}$	total velocity relative to blade
$\bar{\gamma}$	body surface tangential vortex sheet strength
γ	wake tangential vortex sheet strength ($\equiv \gamma_\theta$)
γ_m	wake meridional vortex sheet strength
$\vec{\omega}$	vorticity
B	number of blades per rotor
$c(r)$	blade chord
$c_\ell(r)$	blade section lift coefficient
$c_d(r)$	blade section profile drag coefficient
α_o	blade airfoil zero-lift angle
$\beta(r)$	blade angle
$\phi(r)$	net flow angle relative to blade
$\Gamma(r)$	blade circulation
$\Sigma(r)$	apparent source due to profile drag
Ω	rotor rotational speed

1   Geometry

Figure 1 shows the assumed blade row geometry for rotor or stator, defined in lefthanded cylindrical coordinates. The angle θ is positive about the $-x$ direction, so a conventional righthanded rotor rotates in the $+\theta$ direction.
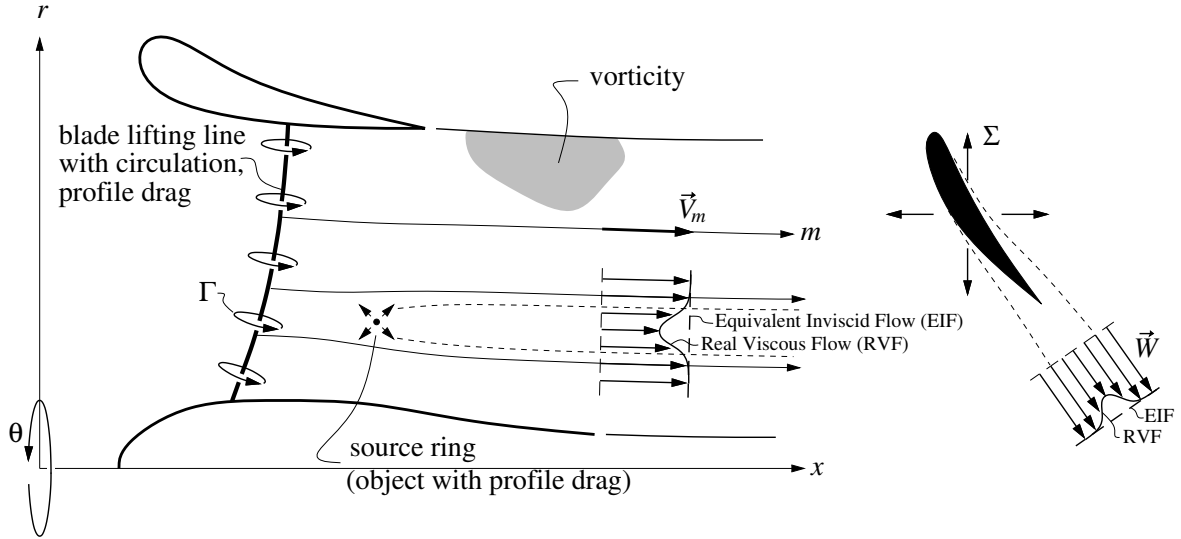

Figure 1: Ducted propulsor geometry with blade lifting line, vortical wake, and profile drag source.

The velocities computed by the present approach will correspond to the Equivalent Inviscid Flow (EIF), which is a locally irrotational continuation into a viscous wake, as shown in Figure 1. This concept allows modeling of drag-producing objects by simple source elements such as a source ring or axisymmetric source panel. The Real Viscous Flow (RVF) velocity, also shown in Figure 1, can be reconstructed if necessary using convected quantities, as will be described later.
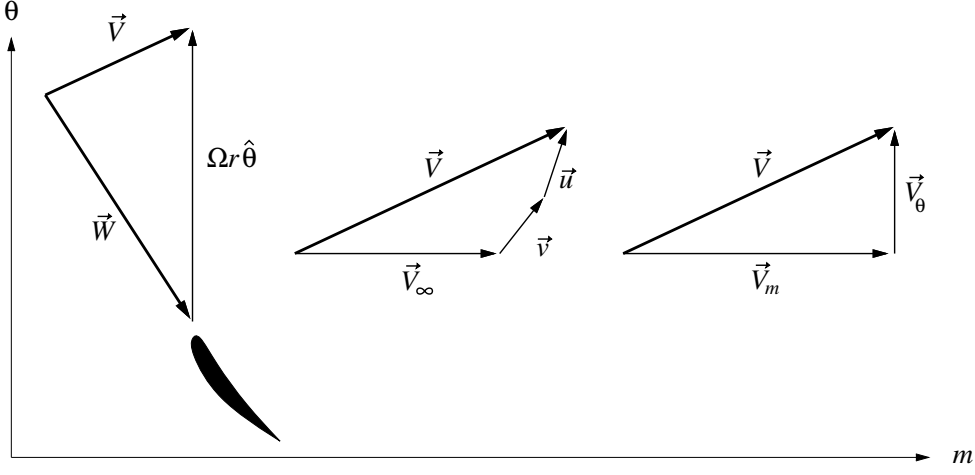
Figure 2: Velocity triangle at one radial blade station and velocity decomposition.

2   Velocity Decomposition

Figure 2 shows the velocity triangle seen by a blade section at radius r. The local velocity $\vec{V}$ relative to the duct is the vector resultant of the freestream velocity V_∞, the induced velocity of the blade row and bodies $\vec{v}$, and any "external" velocity $\vec{u}$. The latter might be due to an upstream rotor or obstruction.

$$\vec{V} \;=\; \vec{v} \,+\, \vec{u} \,+\, V_\infty \hat{x} \tag{1}$$

The local velocity $\vec{W}$ relative to the blade also includes the tangential component from rotor rotation.

$$\vec{W} \;=\; \vec{V} \,-\, \Omega r \,\hat{\theta} \tag{2}$$

The individual velocity components are therefore

$$\begin{aligned}
V_x &= v_x + u_x + V_\infty \\
V_r &= v_r + u_r \\
V_\theta &= v_\theta + u_\theta
\end{aligned} \tag{3}$$

$$\begin{aligned}
W_x &= v_x + u_x + V_\infty \\
W_r &= v_r + u_r \\
W_\theta &= v_\theta + u_\theta - \Omega r
\end{aligned} \tag{4}$$

The meridional velocity $\vec{V}_m$ shown in Figure 1 is defined to be tangent to the mean streamline in the meridional x-r plane,

$$\vec{V}_m \;=\; \vec{W}_m \;=\; V_x \hat{x} \,+\, V_r \hat{r} \tag{5}$$

so that the total velocity vectors can be given only in terms of the m and θ components, as pictured in Figure 2.

$$\vec{V} \;=\; \vec{V}_m \,+\, V_\theta \hat{\theta} \tag{6}$$

$$\vec{W} \;=\; \vec{V}_m \,+\, W_\theta \hat{\theta} \tag{7}$$

3

3 Circulation and Tangential Velocity

Conservation of circulation around a streamtube gives the tangential velocity v_θ explicitly in terms of the net circulation $\tilde{\Gamma}$ of all upstream blade rows intersecting that streamtube, as shown in Figure 3. The circulation contributed by one blade row with B blades each having circulation Γ, is simply $B\Gamma$.

$$v_\theta = \frac{\tilde{\Gamma}}{2\pi r} \tag{8}$$

$$\tilde{\Gamma} = \sum_{\text{upstream}} B\Gamma \tag{9}$$

In some situations it is necessary to obtain the tangential velocity on the blade row itself, e.g. in
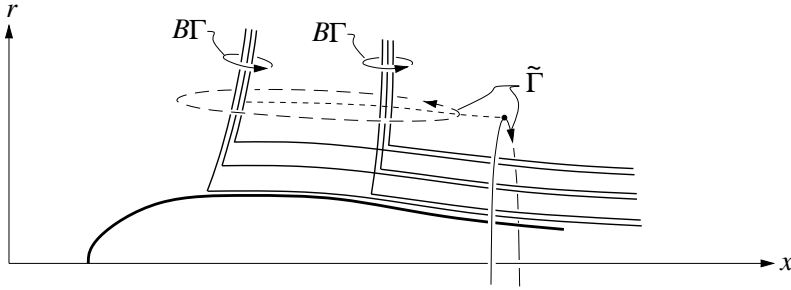

Figure 3: Field circulation $\tilde{\Gamma}$ is sum of circulations of upstream blade rows.

order to relate the blade loading to the local flow angle and blade section properties. In this case that blade row contributes half of its own circulation to its own tangential velocity.

$$(v_\theta)_{\text{row}} = \frac{1}{2\pi r}\left(\tilde{\Gamma} + \frac{1}{2}B\Gamma\right) \tag{10}$$

4 Vorticity Representation

At any blade location where the circulation changes by $\Delta\Gamma$ (including the root and tip), a helical filament of strength $-\Delta\Gamma$ will be shed into the flow. To be force-free, the filaments must be parallel to the total velocity $\vec{W}$ relative to the blade. To allow an axisymmetric treatment, these filaments are smeared into tangential vortex sheets of strength γ_θ, and meridional vortex sheets of strength γ_m, as shown in Figure 4. These strengths are simply the circulation/length densities in the two directions. The θ subscript on γ_θ will be dropped for convenience.

$$\gamma_m = -\frac{B\,\Delta\Gamma}{2\pi r} \tag{11}$$

$$\gamma_\theta \equiv \gamma = -\frac{B\,\Delta\Gamma}{2\pi r}\frac{W_\theta}{W_m} \tag{12}$$

For a field location with some number of upstream blade rows, such as the one shown in Figure 3, the more general form of relation (11) uses the local total circulation jump across the sheet.

$$\gamma_m = -\frac{\Delta\tilde{\Gamma}}{2\pi r} \tag{13}$$

The general expression for γ_θ is obtained from pressure relations, developed in the following sections.
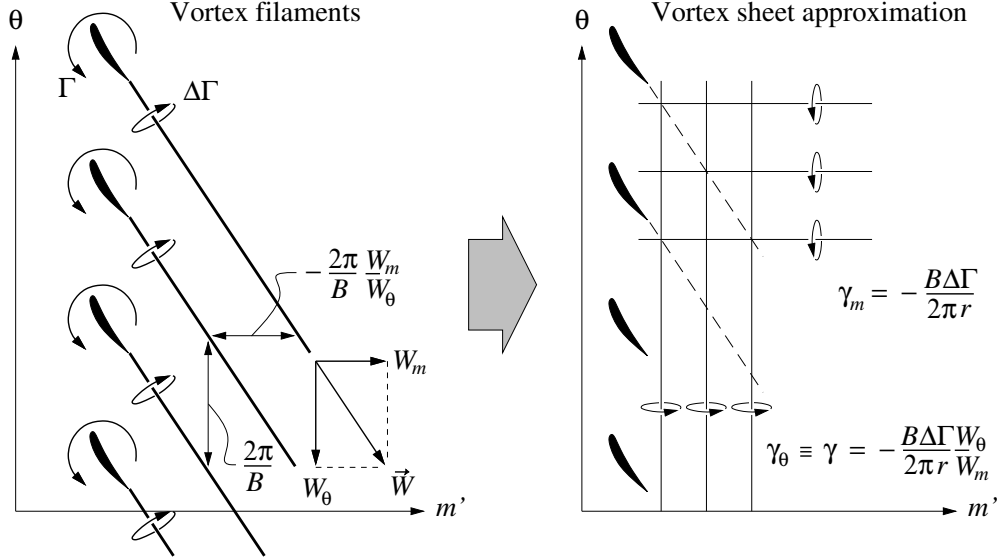
4

Figure 4: Blade circulation change $\Delta\Gamma$ producing helical vortex filaments on an m-θ surface. The filaments are represented by equivalent tangential and meridional vortex sheets γ_θ and γ_m. A negative tangential relative velocity W_θ is shown.

5   Thermodynamic relations

5.1   Total pressure

A rotor, stator, or other obstruction will result in downstream changes in total enthalpy H and entropy s. These must be accompanied by changes in the total pressure p_o, according to the following definition of entropy.

$$s - s_\infty \;\; = \;\; \ln\left[\frac{(H/H_\infty)^{\gamma/(\gamma-1)}}{p_o/p_{o_\infty}}\right] \tag{14}$$

Defining changes relative to the far-upstream values,

$$\tilde{p}_o \;\equiv\; p_o - p_{o_\infty} \qquad\qquad \tilde{H} \;\equiv\; H - H_\infty \qquad\qquad \tilde{s} \;\equiv\; s - s_\infty$$

relation (14) becomes

$$1 + \frac{\tilde{p}_o}{p_{o_\infty}} \;\; = \;\; \left(1 + \frac{\tilde{H}}{H_\infty}\right)^{\gamma/(\gamma-1)} \exp\left(-\tilde{s}\right) \tag{15}$$

For low Mach numbers, it can be assumed that

$$\tilde{p}_o/p_{o_\infty} \;\ll\; 1 \qquad\qquad \tilde{H}/H_\infty \;\ll\; 1 \qquad\qquad \tilde{s} \;\ll\; 1$$

which simplifies (15) to the following.

$$\tilde{p}_o \;\; \simeq \;\; \rho\left(\tilde{H} - \tilde{S}\right) \tag{16}$$

$$\tilde{S} \;\; \equiv \;\; \frac{p}{\rho}\,\tilde{s} \tag{17}$$

At low Mach numbers p/ρ is very nearly constant, in which case it is valid to treat $\tilde{S}$ as the convected quantity rather than $\tilde{s}$.

5

5.2   Disk jump conditions

After the periodic flow about the rotor blades is averaged in θ, there will generally be a change in the total enthalpy H across the rotor disk as a result of the work done on the fluid. Similarly, there will be a change in entropy across a friction-producing disk, ideally modeled as a screen with friction coefficient C_f. Figure 5 shows two points immediately in front and behind the rotor or friction disk.
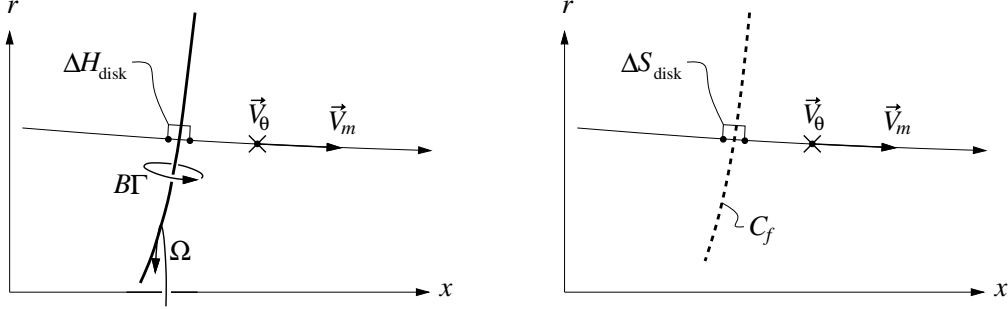

Figure 5: Jumps across a loaded rotor disk and resistive screen.

The jump relations are

$$\Delta H_{\text{disk}} = \Omega \, \Delta(rV_\theta) = \Omega \, \frac{B\Gamma}{2\pi} \tag{18}$$

$$\Delta S_{\text{disk}} = \frac{1}{2} V_m^2 \, C_f \tag{19}$$

and the values $\tilde{H}$ and $\tilde{S}$ at any field point are the accumulated jumps of all the upstream blade rows or obstructions. These are computed the same way as the circulation, as shown in Figure 3.

$$\tilde{H} = \sum_{\text{upstream}} \Delta H_{\text{disk}} \tag{20}$$

$$\tilde{S} = \sum_{\text{upstream}} \Delta S_{\text{disk}} \tag{21}$$

5.3   Static pressure — Bernoulli equation

According to (16), the total pressure p_o at any point is equal to the freestream value p_{o_∞}, plus upstream work and loss contributions. The static pressure then follows from the Bernoulli equation.

$$p_o = p_{o_\infty} + \rho(\tilde{H} - \tilde{S}) \tag{22}$$

$$p = p_{o_\infty} - \frac{1}{2}\rho V^2 + \rho\left(\tilde{H} - \tilde{S}\right) \qquad \text{(RVF velocity)} \tag{23}$$

As indicated, (23) assumes that V is the velocity of the Real Viscous Flow. Obtaining this RVF requires representation of all the vorticity present, including that in viscous wakes. An alternative and simpler approach is to treat the Equivalent Inviscid Flow velocity, by using a source sheet at the drag element itself, with no trailing vortex sheets. Figure 6 compares the two approaches. To obtain the pressure in the EIF model, the entropy is simply excluded from the total pressure.

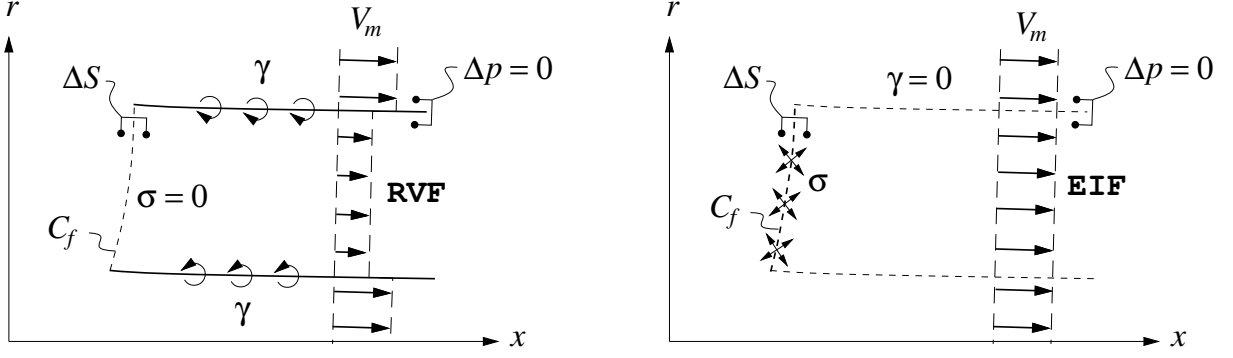$$p = p_{o_\infty} - \frac{1}{2}\rho V^2 + \rho \tilde{H} \qquad \text{(EIF velocity)} \tag{24}$$

6

Figure 6: Two alternative representations of a drag-producing object.

Either approach will correctly predict a zero pressure jump, $\Delta p = 0$, across the vortex sheet or bounding streamline.

6 Rotor vortex sheet jump relations

6.1 Velocity jumps

Figure 7 shows velocities on the two sides of a vortex sheet trailing from one rotor radial station. The sheet strengths are defined in terms of these velocities, using relations shown in Figure 4, and the swirl/circulation relation (8), with $\tilde{\Gamma} = B\Gamma$ for the single rotor. We're assuming that no additional vorticity is created by blade profile drag, so that the velocities in this case represent EIF.

$$\gamma_m \;=\; V_{\theta_1} - V_{\theta_2} \;\;=\;\; -\frac{B(\Gamma_2 - \Gamma_1)}{2\pi r} \tag{25}$$

$$\gamma \;\equiv\; \gamma_\theta \;=\; V_{m_2} - V_{m_1} \;\;=\;\; -\frac{B(\Gamma_2 - \Gamma_1)}{2\pi r} \frac{W_{\theta_\text{avg}}}{W_{m_\text{avg}}} \tag{26}$$
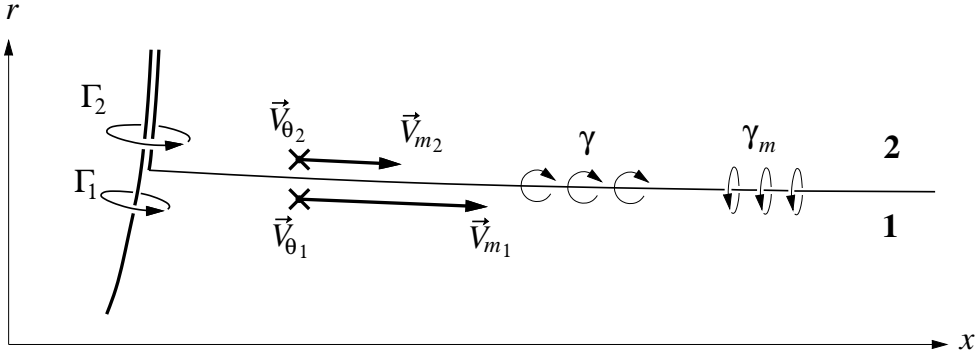

Figure 7: Velocities on the two sides of a vortex sheet shed by rotor.

The sheet-average velocities are defined as follows.

$$W_{\theta_\text{avg}} \;\equiv\; \frac{1}{2}\left(W_{\theta_1} + W_{\theta_2}\right) \;=\; \frac{1}{2}\left(V_{\theta_1} + V_{\theta_2}\right) \;-\; \Omega r \tag{27}$$

$$W_{m_\text{avg}} \;\equiv\; \frac{1}{2}\left(W_{m_1} + W_{m_2}\right) \;=\; \frac{1}{2}\left(V_{m_1} + V_{m_2}\right) \tag{28}$$

7

Combining equations (25) and (26) gives

$$W_{m_{\mathrm{avg}}}\gamma_\theta - W_{\theta_{\mathrm{avg}}}\gamma_m = 0 \tag{29}$$

$$V_{m_{\mathrm{avg}}}\gamma_\theta - \left(V_{\theta_{\mathrm{avg}}} - \Omega r\right)\gamma_m = 0 \tag{30}$$

$$\frac{1}{2}\left(V_2^2 - V_1^2\right) = \Omega\frac{B(\Gamma_2 - \Gamma_1)}{2\pi} \tag{31}$$

where $V^2 = V_m^2 + V_\theta^2$ is the total velocity magnitude. We also note that the sheet strengths can be defined as

$$\gamma_m = W_{\theta_1} - W_{\theta_2} \tag{32}$$

$$\gamma_\theta = W_{m_2} - W_{m_1} \tag{33}$$

which can be combined with (29) to give

$$\frac{1}{2}\left(W_2^2 - W_1^2\right) = 0 \tag{34}$$

$$|W_2| = |W_1| \tag{35}$$

6.2   Sheet pressure jump

Using the Bernoulli equation (23), the static pressure jump across the sheet is then given by one of the following relations.

$$p_2 - p_1 = -\frac{1}{2}\rho\left(V_2^2 - V_1^2\right) + \rho\left(\tilde{H}_2 - \tilde{H}_1 - \tilde{S}_2 + \tilde{S}_1\right) \qquad \text{(RVF)} \tag{36}$$

$$p_2 - p_1 = -\frac{1}{2}\rho\left(V_2^2 - V_1^2\right) + \rho\left(\tilde{H}_2 - \tilde{H}_1\right) \qquad \text{(EIF)} \tag{37}$$

Combining this with the $\tilde{H}$ definitions (18) and (20), and the sheet velocity jump condition (31), gives

$$p_2 - p_1 = 0 \tag{38}$$

as expected from physical considerations.

7   Tangential Vortex Sheet Strength

The tangential vortex sheet strength γ immediately behind a rotor is defined by relation (12). This relation is not appropriate for using at an arbitrary location in the field, since the Ωr component of W_θ is then ill-defined. Instead, we will use the alternative and equivalent condition that the sheet pressure jump as given by (37) is zero. Assuming the EIF representation (37) for illustration, setting $p_2 - p_1 = 0$ gives

$$\frac{1}{2}\left(V_2^2 - V_1^2\right) = \tilde{H}_2 - \tilde{H}_1 \tag{39}$$

$$V_{m_2}^2 - V_{m_1}^2 + V_{\theta_2}^2 - V_{\theta_1}^2 = 2\left(\tilde{H}_2 - \tilde{H}_1\right) \tag{40}$$

$$V_{m_2}^2 - V_{m_1}^2 = -\left(\frac{1}{2\pi r}\right)^2\left(\tilde{\Gamma}_2^2 - \tilde{\Gamma}_1^2\right) + 2\left(\tilde{H}_2 - \tilde{H}_1\right) \tag{41}$$

Equation (41) can be used in two ways to determine the vortex sheet strength from a specified $\tilde{\Gamma}$ and $\tilde{H}$ field. If V_{m_2} is known, we can determine V_{m_1} from (41), and the sheet strength then follows.

$$\gamma \;\; = \;\; V_{m_2} - V_{m_1} \tag{42}$$

Equations (41) and (42) can be marched radially inward at one streamwise location. The march is started just outside the outermost sheet, where V_{m_2} is known (e.g. $V_m \simeq V_\infty$). For each sheet, V_{m_1} and γ are computed. This V_{m_1} is then also assumed to equal the V_{m_2} value for next inside sheet. In effect, the V_m velocity profile is assumed to be constant between vortex sheets.

If instead the sheet $V_{m_{\mathrm{avg}}}$ is known, equation (41) can be recast as an explicit expression for γ.

$$V_{m_{\mathrm{avg}}} \;\; = \;\; \frac{1}{2}\left(V_{m_1} + V_{m_2}\right) \tag{43}$$

$$V_{m_2}^2 \;\; - \;\; V_{m_1}^2 \;\; = \;\; 2 V_{m_{\mathrm{avg}}}\,\gamma \tag{44}$$

$$\gamma \;\; = \;\; \frac{1}{V_{m_{\mathrm{avg}}}}\left[-\frac{1}{2}\left(\frac{1}{2\pi r}\right)^2\left(\tilde{\Gamma}_2^2 - \tilde{\Gamma}_1^2\right) \;+\; \tilde{H}_2 - \tilde{H}_1\right] \tag{45}$$

8 Vortex Sheet Discretization

The induced velocity $\vec{v}$ is the result of the duct and center bodies, the trailing vorticity, and viscous displacement effects. The effect of the bodies is represented by tangential vortex sheets of strength $\bar{\gamma}$ placed on the body surfaces (the θ subscript on γ is omitted for convenience). The effect of the trailing vorticity is represented by the tangential and meridional vortex sheets of strengths γ and γ_m, as shown in Figure 4. Viscous displacement is represented by source sheets of strength σ. Figure 8 shows the various sheets on the geometry.
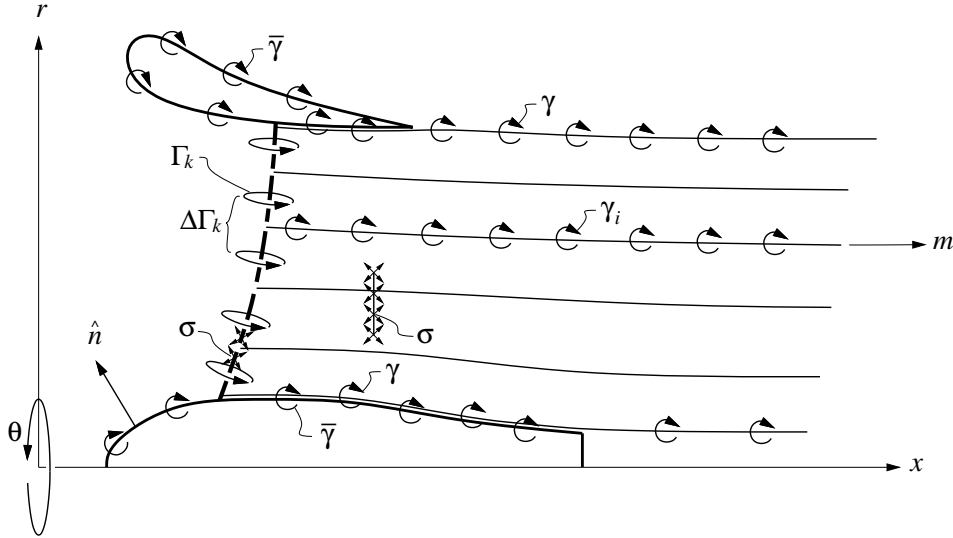

Figure 8: Vortex sheets used to represent meridional velocity $\vec{V}_m$.

The continuous sheet strengths will now be approximated via discrete panel-node values $\bar{\gamma}_i$, γ_i, and σ_i. The induced velocity components at any location i are then given via influence matrices.

$$v_{x_i} \;\; = \;\; \bar{a}_{x_{ij}}\bar{\gamma}_j \;+\; a_{x_{ij}}\gamma_j \;+\; b_{x_{ij}}\sigma_j \tag{46}$$

$$v_{r_i} \;\; = \;\; \bar{a}_{r_{ij}}\bar{\gamma}_j \;+\; a_{r_{ij}}\gamma_j \;+\; b_{r_{ij}}\sigma_j \tag{47}$$

9

The tangential induced velocity is given directly in terms of the local circulation of all upstream blade rows.

$$v_{\theta_i} = \frac{\tilde{\Gamma}_i}{2\pi r_i} \tag{48}$$

9 Body vorticity elimination

As in any panel method, the body vortex sheet strengths $\bar{\gamma}_i$ are constrained by the flow tangency boundary condition.

$$\vec{V}_i \cdot \hat{n}_i = 0 \tag{49}$$

This can be written as

$$\bar{a}_{ij}\bar{\gamma}_j + a_{ij}\gamma_j + b_{ij}\sigma_j + V_\infty n_{x_i} = 0 \tag{50}$$

where

$$\bar{a}_{ij} = \bar{a}_{x_{ij}} n_{x_i} + \bar{a}_{r_{ij}} n_{r_i} \tag{51}$$

$$a_{ij} = a_{x_{ij}} n_{x_i} + a_{r_{ij}} n_{r_i} \tag{52}$$

$$b_{ij} = b_{x_{ij}} n_{x_i} + b_{r_{ij}} n_{r_i} \tag{53}$$

Factoring the $\bar{a}_{ij}$ matrix then gives $\bar{\gamma}$ explicitly as follows.

$$\bar{\gamma}_i = \bar{\gamma}_{o_i} V_\infty + a'_{ij}\gamma_j + b'_{ij}\sigma_j \tag{54}$$

$$\bar{\gamma}_{o_i} \equiv -\bar{a}_{ij}^{-1} n_{x_j} \tag{55}$$

$$a'_{ij} \equiv -\bar{a}_{i\ell}^{-1} a_{\ell j} \tag{56}$$

$$b'_{ij} \equiv -\bar{b}_{i\ell}^{-1} b_{\ell j} \tag{57}$$

The freestream-influence vector $\bar{\gamma}_{o_i}$ and source-influence matrix b'_{ij} depend only on the body and source panel geometry, and hence can be precomputed and stored. The wake-influence matrix a'_{ij} depends also on the wake's constant-m surface shapes, which in turn depend on the freestream speed as well as the rotor loading.

The meridional induced velocities can now be given only in terms of the freestream speed V_∞, the source sheet strengths σ_i, and the wake vortex sheet strengths γ_i.

$$v_{x_i} = \bar{a}_{x_{ij}}\bar{\gamma}_{o_j} V_\infty + \left[\bar{a}_{x_{i\ell}} b'_{\ell j} + b_{x_{ij}}\right]\sigma_j + \left[\bar{a}_{x_{i\ell}} a'_{\ell j} + a_{x_{ij}}\right]\gamma_j \tag{58}$$

$$v_{r_i} = \bar{a}_{r_{ij}}\bar{\gamma}_{o_j} V_\infty + \left[\bar{a}_{r_{i\ell}} b'_{\ell j} + b_{r_{ij}}\right]\sigma_j + \left[\bar{a}_{r_{i\ell}} a'_{\ell j} + a_{r_{ij}}\right]\gamma_j \tag{59}$$

It should be pointed out that the cost of evaluating the sums in (58) and (59) strongly depends on the evaluation order of the matrix-matrix-vector products. For example, the last such term in (58) should be evaluated left to right,

$$\bar{a}_{x_{i\ell}} a'_{\ell j} \gamma_j = -\bar{a}_{x_{i\ell}} \bar{a}_{i\ell}^{-1} a_{\ell j} \gamma_j = -\bar{a}_{x_{i\ell}} \left\{\bar{a}_{i\ell}^{-1} \left\{a_{\ell j} \gamma_j\right\}\right\} \tag{60}$$

which requires only matrix-vector products. A right to left evaluation order would require vastly more expensive matrix-matrix products.

10   Blade Load Representation

The wake vortex sheet strength is related to the circulation and total enthalpy jumps across the sheet, via relation (45).

$$\gamma_i \;=\; \frac{1}{V_{m_i}}\left[-\frac{1}{2}\left(\frac{1}{2\pi r}\right)^2 \Delta\big(\tilde{\Gamma}^2\big) \;+\; \Delta\big(\tilde{H}_i\big)\right] \tag{61}$$

Both $\tilde{\Gamma}$ and $\tilde{H}$ are functions of the individual blade station circulations Γ_k. Substitution into equations (46) and (47) then gives the meridional induced velocities only in terms of V_∞, the drag sources σ_i, and the blade circulations Γ_k.

$$v_{x_i} \;=\; v_{xo_i}\,V_\infty \;+\; B_{x_{ij}}\sigma_j \;+\; A_{x_{ik}}\gamma_j(V_\infty,\sigma_j,\Gamma_k) \tag{62}$$

$$v_{r_i} \;=\; v_{ro_i}\,V_\infty \;+\; B_{r_{ij}}\sigma_j \;+\; A_{r_{ik}}\gamma_j(V_\infty,\sigma_j,\Gamma_k) \tag{63}$$

$$v_{xo_i} \;=\; \bar{a}_{x_{ij}}\bar{\gamma}_{o_j} \tag{64}$$

$$v_{ro_i} \;=\; \bar{a}_{r_{ij}}\bar{\gamma}_{o_j} \tag{65}$$

$$B_{x_{ij}} \;=\; \bar{a}_{x_{i\ell}}b'_{\ell j} \;+\; b_{x_{ij}} \tag{66}$$

$$B_{r_{ij}} \;=\; \bar{a}_{r_{i\ell}}b'_{\ell j} \;+\; b_{r_{ij}} \tag{67}$$

$$A_{x_{ij}} \;=\; \bar{a}_{x_{i\ell}}a'_{\ell j} \;+\; a_{x_{ij}} \tag{68}$$

$$A_{r_{ij}} \;=\; \bar{a}_{r_{i\ell}}a'_{\ell j} \;+\; a_{r_{ij}} \tag{69}$$

The nonlinear $\gamma_j(V_\infty,\sigma_j,\Gamma_k)$ function is given by equation (61).

The remaining tangential induced velocity defined by equation (48) can be put into the same form, except that it has no V_∞ or σ_j dependence.

$$v_{\theta_i} \;=\; A_{\theta_{ik}}\Gamma_k \tag{70}$$

$$A_{\theta_{ik}} \;\equiv\; \begin{cases} \dfrac{B}{4\pi\,r_i} & , \quad [i \in i(k), i(k{-}1)] \\[2mm] 0 & , \quad [i \notin i(k), i(k{-}1)] \end{cases} \tag{71}$$

11   Viscous Drag Equivalent Source

11.1   Blade profile drag

The rotor blade profile drag/span $\Sigma_{(r)}$ is given by

$$\Sigma \;=\; \frac{1}{2}\,W c\, c_d \tag{72}$$

This is represented by an axisymmetric source sheet placed on the rotor disk. The sheet strength σ at some radius r is obtained by smearing the total source/span strength of all the blades around the local circumference.

$$\sigma \;=\; \frac{B\Sigma}{2\pi r} \;=\; \frac{B}{4\pi r}\,W c\, c_d \tag{73}$$

11.2 Stationary object profile drag

The source strength σ needed to represent the displacement effect of an object's viscous wake is related to the drag by

$$D = \rho V_m \sigma A$$

where A is the area of the source sheet. The drag is most conveniently represented by a drag area A_D, so that

$$\sigma = \frac{D}{\rho V_m A} = \frac{1}{2} V_m \frac{A_D}{A} \tag{74}$$

The object being modeled is assumed to be axisymmetric, so that discrete objects such as cylinder heads must be represented by an equivalent axisymmetric obstruction of similar total A_D. This model also assumes that the mass defect of the trailing wake does not vary significantly downstream of the object, which is a good approximation if the streamwise pressure gradients along the wake are modest. The worst case situation would be a massive blockage due to viscous wake bursting in a strong adverse pressure gradient. Modeling this would require placing source panels all along the wake, and varying their strength in accordance with the wake displacement area as governed by strongly interacting boundary layer equations. This level of blockage modeling is beyond the scope of the present analysis approach.

In the source strength expressions (73) and (74), the drag coefficient c_d and drag area A_D can usually be specified explicitly, but the local velocities W and V_m will depend on the overall flow solution. Hence, σ will depend not only on V_∞, but also on the entire rotor circulation distribution Γ_j. The most reliable solution approach is to include σ as an unknown in the overall Newton system.

12 Blade Section Relations

The rotor blade is represented as a lifting line, with a circulation $\Gamma_{(r)}$.

$$\Gamma = \frac{1}{2} W c \, c_\ell \tag{75}$$

The section lift coefficient c_ℓ depends on the local aerodynamic angle of attack, as shown in Figure 9.

$$c_\ell = m_{2D} \left(\beta - \phi - \alpha_o \right) \tag{76}$$

$$\phi = \arctan \frac{W_m}{-W_\theta} = \arctan \frac{V_\infty + v_m + u_m}{\Omega r - v_\theta - u_\theta} \tag{77}$$

Application of equation (75) to all blade radial stations $i = 1 \ldots N$, and elimination of v_m and v_θ in (77) in terms of Γ_j, produces an $N \times N$ system for all the Γ_i strengths. If source sheets are present, the system can be augmented by including the strengths σ_i as additional unknowns, with (73) or (74) for each source sheet node being the corresponding equations. If σ_i are expected to have a small effect, they can be set explicitly after each Newton iteration, although this will of course degrade the Newton convergence of Γ_i by some degree.

13 Axisymmetric wake geometry

The vortex filaments and vortex sheets shown in Figure 4 lie on axisymmetric streamsurfaces parallel to the meridional velocity $\vec{V}_m$. One approach to computing these surfaces would be to
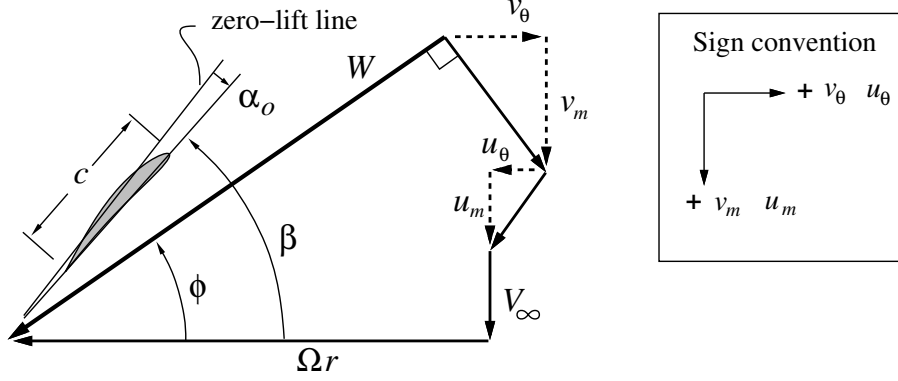
Figure 9: Blade-section velocities and angles

integrate the streamlines defined by $\vec{V}_m$. However, in the context of a panel method, this is an expensive proposition. An alternative approach, which will be taken here, is to use an elliptic grid generation method.

13.1   Axisymmetric streamfunction

First we consider the axisymmetric streamfunction $\psi(x,r)$, which defines the velocity components as

$$V_x \;\; = \;\; \frac{1}{\rho r}\frac{\partial \psi}{\partial r} \tag{78}$$

$$V_r \;\; = \;\; \frac{-1}{\rho r}\frac{\partial \psi}{\partial x} \tag{79}$$

where ρ is the air density. These velocity components identically satisfy the continuity equation.

$$\frac{\partial(\rho r V_x)}{\partial x} \;\; + \;\; \frac{\partial(\rho r V_r)}{\partial r} \;\; = \;\; 0$$

Evaluation of the circumferential vorticity gives

$$\omega_\theta \;\; \equiv \;\; \frac{\partial V_x}{\partial r} \;-\; \frac{\partial V_r}{\partial x} \;\; = \;\; \frac{1}{\rho r}\left(\psi_{xx} + \psi_{rr}\right) \;+\; \psi_x \left(\frac{1}{\rho r}\right)_x \;+\; \psi_r \left(\frac{1}{\rho r}\right)_r \tag{80}$$

which can be written as a Poisson equation for ψ.

$$\psi_{xx} + \psi_{rr} \;\; = \;\; \frac{1}{r}\psi_r \;+\; r(\vec{V}_m \times \nabla\rho)\cdot\left(-\hat{\theta}\right) \;+\; \rho r \omega_\theta \tag{81}$$

The steady Crocco relation is

$$\vec{V} \times \vec{\omega} \;\; = \;\; \nabla\tilde{H} \;-\; \nabla\tilde{S}$$

$$V_m\,\omega_\theta \;-\; V_\theta\,\omega_m \;\; = \;\; \frac{\partial\tilde{H}}{\partial n} - \frac{\partial\tilde{S}}{\partial n} \tag{82}$$

13

We note that

$$V_\theta = \frac{\tilde{\Gamma}}{2\pi r}$$

$$\omega_m = -\frac{1}{r}\frac{\partial(rV_\theta)}{\partial n} = -\frac{1}{2\pi r}\frac{\partial\tilde{\Gamma}}{\partial n}$$

$$V_\theta\,\omega_m = -\frac{1}{2}\left(\frac{1}{2\pi r}\right)^2\frac{\partial(\tilde{\Gamma}^2)}{\partial n} \tag{83}$$

so that (82) becomes

$$V_m\,\omega_\theta = -\frac{1}{2}\left(\frac{1}{2\pi r}\right)^2\frac{\partial(\tilde{\Gamma}^2)}{\partial n} + \frac{\partial\tilde{H}}{\partial n} - \frac{\partial\tilde{S}}{\partial n} \tag{84}$$

Then using relation (84) to replace the ω_θ term from (81) gives the final Poisson equation governing $\psi(x,r)$.

$$\psi_{xx} + \psi_{rr} = Q_0 + Q_1 \tag{85}$$

$$Q_0 = \frac{1}{r}\psi_r \tag{86}$$

$$Q_1 = \rho r\left[\frac{\vec{V}_m \times \nabla\rho}{\rho} - \frac{1}{2}\left(\frac{1}{2\pi r}\right)^2\frac{\vec{V}_m \times \nabla(\tilde{\Gamma}^2)}{V_m^2} + \frac{\vec{V}_m \times \nabla\tilde{H}}{V_m^2} - \frac{\vec{V}_m \times \nabla\tilde{S}}{V_m^2}\right]\cdot\left(-\hat{\theta}\right) \tag{87}$$

The first source term Q_0 is simply from the axisymmetry of the problem. The four terms in the second source term Q_1 represent the density dilatation effect of compressibility, the transverse circulation gradient, the transverse work gradient, and the transverse loss gradient, respectively. In low speed flow, $\nabla\rho$ is negligible, and the following Q_1 definition can then be employed.

$$Q_1 = \frac{\rho r}{V_m^2}\left[\frac{1}{2}\left(\frac{1}{2\pi r}\right)^2\vec{V}_m \times \nabla(\tilde{\Gamma}^2) + \vec{V}_m \times \nabla\tilde{H} - \vec{V}_m \times \nabla\tilde{S}\right]\cdot\left(-\hat{\theta}\right) \tag{88}$$

Note that $-\hat{\theta}$ points out of the x-r plane.

13.2 Grid equations

The grid shown in Figure 10 is defined parametrically by the functions

$$x(\xi,\eta)\ ,\quad r(\xi,\eta) \qquad\text{or}\qquad \xi(x,r)\ ,\quad \eta(x,r)$$

where ξ is constant along each quasi-radial line, and η is constant along each streamline. The functions are chosen to be governed by Poisson equations.

$$\xi_{xx} + \xi_{rr} = P \tag{89}$$

$$\eta_{xx} + \eta_{rr} = Q \tag{90}$$

By setting

$$Q = Q_0 + Q_1 \tag{91}$$

we make (90) identical to (85), so that $\eta = \psi$ and the constant-η lines of the grid correspond to physical streamlines. The ξ coordinate has no physical interpretation, and its source term P is somewhat arbitrary. It is workable to simply set $P = 0$.
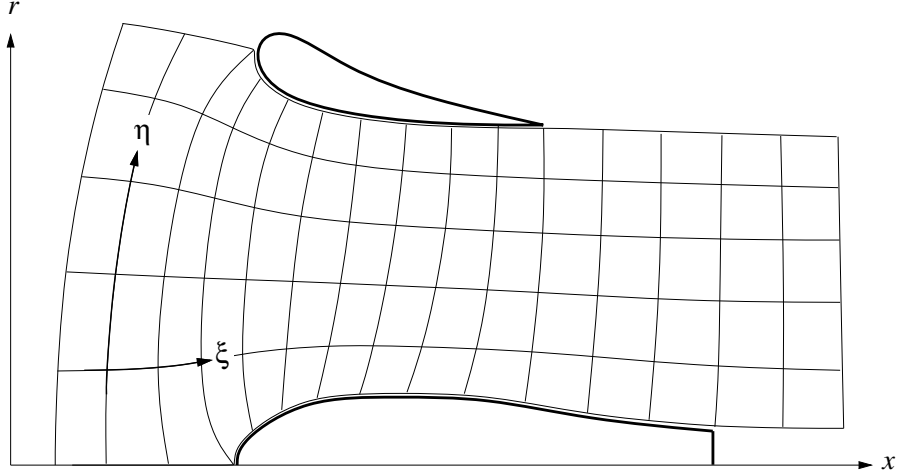
Figure 10: Grid and grid parameters.

Following the procedure of Thompson [3], equations (89) and (90) are inverted to give

$$\alpha x_{\xi\xi} - 2\beta x_{\xi\eta} + \frac{1}{r}\gamma\left(rx_\eta\right)_\eta - \frac{1}{r}\beta r_\xi x_\eta + J^2 r Q_1 x_\eta = 0 \tag{92}$$

$$\alpha r_{\xi\xi} - 2\beta r_{\xi\eta} + \frac{1}{r}\gamma\left(rr_\eta\right)_\eta - \frac{1}{r}\beta r_\xi r_\eta + J^2 r Q_1 r_\eta = 0 \tag{93}$$

where

$$\alpha = x_\eta^2 + r_\eta^2 \tag{94}$$
$$\gamma = x_\xi^2 + r_\xi^2 \tag{95}$$
$$\beta = x_\xi x_\eta + r_\xi r_\eta \tag{96}$$
$$J = x_\xi r_\eta - x_\eta r_\xi \tag{97}$$

The two differential indentities of the transformation are

$$\begin{bmatrix} x_\xi & x_\eta \\ r_\xi & r_\eta \end{bmatrix} \begin{Bmatrix} d\xi \\ d\eta \end{Bmatrix} = \begin{Bmatrix} dx \\ dr \end{Bmatrix} \tag{98}$$

$$\begin{bmatrix} \xi_x & \xi_r \\ \eta_x & \eta_r \end{bmatrix} \begin{Bmatrix} dx \\ dr \end{Bmatrix} = \begin{Bmatrix} d\xi \\ d\eta \end{Bmatrix} \tag{99}$$

Inverting the first identity (98) gives

$$\begin{Bmatrix} d\xi \\ d\eta \end{Bmatrix} = \frac{1}{J} \begin{bmatrix} r_\eta & -x_\eta \\ -r_\xi & x_\xi \end{bmatrix} \begin{Bmatrix} dx \\ dr \end{Bmatrix} \tag{100}$$

and comparing this to the second identity (99) we see that

$$\xi_x = r_\eta/J \tag{101}$$
$$\xi_r = -x_\eta/J \tag{102}$$
$$\eta_x = -r_\xi/J \tag{103}$$
$$\eta_r = x_\xi/J \tag{104}$$

15

Hence the velocities can be computed as follows.

$$u = \frac{\eta_r}{\rho r} = \frac{x_\xi}{\rho r J} \tag{105}$$

$$v = \frac{-\eta_x}{\rho r} = \frac{r_\xi}{\rho r J} \tag{106}$$

With a ξ or η value assigned to each grid line, equations (92) and (93) can then be solved for the node x, r positions. The appropriate boundary conditions are

On solid walls: x, r fixed (Dirichlet condition)
On streamlines: $u^2 + v^2$ fixed (Neumann condition)
On inlet/outlet planes: $u^2 + v^2$ fixed (Neumann condition)

SLOR is a fast and effective solution method. The grid streamlines then provide the geometry of the wake vortex sheets needed to define the overall velocity field.

13.3   Source term evaluation

The source term Q_1 which appears in equations (92) and (93) is evaluated using its definition (88).

Figure 11 shows an element of the rotor imparting a change in total enthalpy ΔH to its streamtube of mass flow $\dot{m}_s$. We also allow for the possibility of rotor blade profile drag $\mathcal{D}_p$ along the relative flow velocity W (not shown), imparting an entropy increase ΔS to the streamtube. A nonlifting object with drag $\mathcal{D}$, represented by the source ring, imparts only entropy. These quantities are
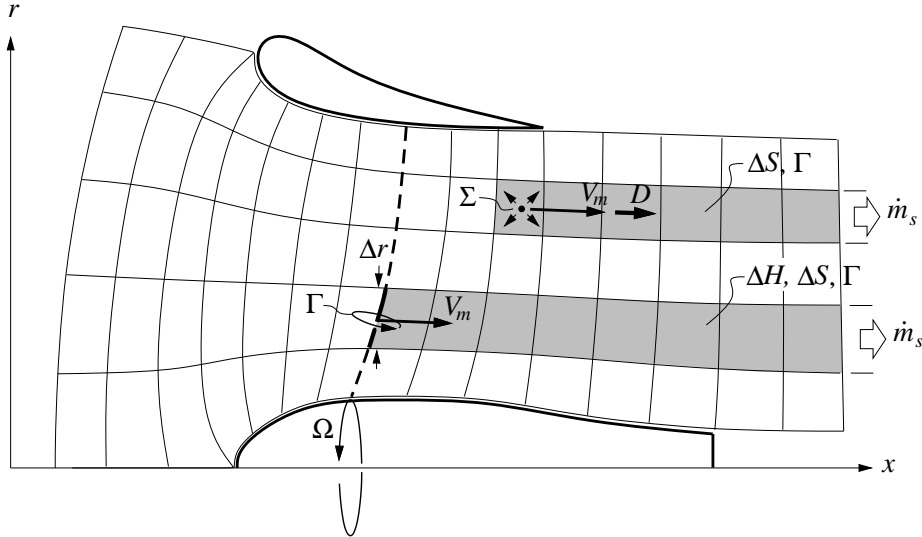

Figure 11: Total enthalpy and entropy source elements.

given by

$$\dot{m}_s = \rho V_m A$$

$$\mathcal{Q} = \rho V_m B \Gamma \, r \, \Delta r = \rho V_m A \, B\Gamma/2\pi$$

$$\mathcal{D} = \frac{1}{2}\rho V_m^2 \, A_D$$

$$\mathcal{D}_p = \frac{1}{2}\rho W^2 \, B \, c \, \Delta r \, c_{d_p}$$

where $A = 2\pi r \Delta r$ is the area of the annular captured streamtube, and A_D is the annular object's profile drag area. The flow jumps produced by the object are given by

$$\dot{m}_s \, \Delta H \;=\; \Omega \, \mathcal{Q} \tag{107}$$

$$\dot{m}_s \, \Delta S \;=\; V_m \, \mathcal{D} \;+\; W \, \mathcal{D}_p \tag{108}$$

There will also be some additional ΔH and ΔS if the object delivers heat, as in the case of a cylinder head or radiator. But the effect of this heating on the flowfield is not likely to be significant in typical applications, and will not be considered here. Substituting for $\dot{m}_s$, $\mathcal{D}$, $\mathcal{D}_p$, and $\mathcal{Q}$ in (107) and (108), gives the final expressions for the convected quantities needed to evaluate the Q_1 source term using (88).

$$\Delta H \;=\; \Omega \, \frac{B\Gamma}{2\pi} \tag{109}$$

$$\Delta S \;=\; \frac{1}{2} V_m^2 \, \frac{A_D}{A} \;+\; \frac{1}{2} \frac{W^3}{V_m} \frac{Bc}{2\pi r} \, c_{d_p} \tag{110}$$

14 Blade Geometry

14.1 Parameterization

The blade chord surface is defined using two parameters ξ, η as shown in Figure 12. The range of the chordwise parameter ξ is assumed to be

$$0 \leq \xi \leq 1$$

from leading edge to trailing edge. The range of the radial parameter η is arbitrary. Two simple and convenient definitions are

$$\eta = r \qquad \text{or} \qquad \eta = (r - r_{\text{root}})/(r_{\text{tip}} - r_{\text{root}})$$

The blade airfoil sections are defined on constant-r (and constant-η) cylinders. A third parameter ζ is used to define the airfoil shape on this cylinder. The ξ lines are helixes with a helix angle of β from the circumferential direction. The ζ lines are the orthogonal helixes with a helix angle of $\beta - 90°$ (not shown).

Both ξ and ζ have the same normalization with the local chord $c(\eta)$, so that a physical arc length Δs on the unwrapped airfoil cylinder is

$$\Delta s \;=\; c \sqrt{\Delta\xi^2 + \Delta\zeta^2}$$

The increments do not have to be small.

14.2 Blade geometry specification

The blade chord surface shape is specified by the following quantities:

$\bar{r}(\eta)$ radius
$\bar{\theta}(\eta)$ skew
$\bar{x}(\eta)$ rake
$c(\eta)$ chord
$\beta(\eta)$ twist
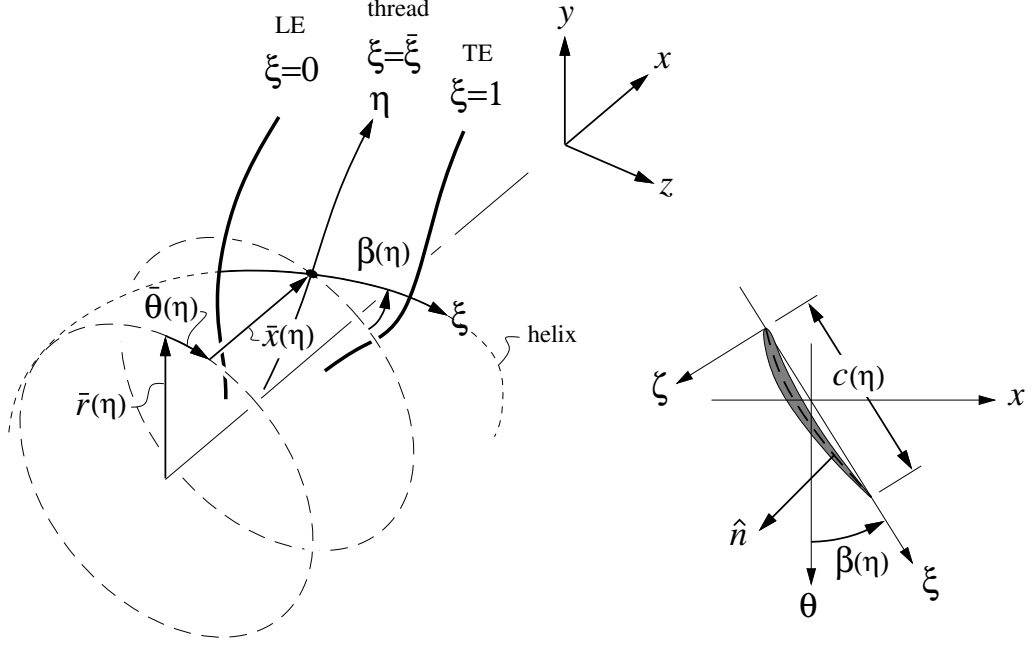$\bar{\xi}(\eta)$ thread position

Figure 12: Blade geometry parameterization.

There will also be an airfoil shape and corresponding camber surface defined in the ξ-ζ plane at each η station.

It is convenient to also work in the cartesian coordinates (x, y, z) shown in Figure 12. Any given point (ξ, η, ζ) on the blade has the following (x, y, z) location.

$$x_{(\xi,\eta,\zeta)} = \bar{x} + c\left[(\xi - \bar{\xi})\sin\beta - \zeta\cos\beta\right] \tag{111}$$

$$y_{(\xi,\eta,\zeta)} = \bar{r}\cos\left\{\bar{\theta} + \frac{c}{r}\left[(\xi - \bar{\xi})\sin\beta - \zeta\cos\beta\right]\right\} \tag{112}$$

$$z_{(\xi,\eta,\zeta)} = \bar{r}\sin\left\{\bar{\theta} + \frac{c}{r}\left[(\xi - \bar{\xi})\sin\beta - \zeta\cos\beta\right]\right\} \tag{113}$$

Defining $\tilde{\zeta}(\xi; \eta)$ as the set of airfoil camberlines for all radii, the corresponding cartesian-coordinate camber surface is

$$\tilde{x}_{(\xi,\eta)} = \bar{x} + c\left[(\xi - \bar{\xi})\sin\beta - \tilde{\zeta}\cos\beta\right] \tag{114}$$

$$\tilde{y}_{(\xi,\eta)} = \bar{r}\cos\left\{\bar{\theta} + \frac{c}{r}\left[(\xi - \bar{\xi})\sin\beta - \tilde{\zeta}\cos\beta\right]\right\} \tag{115}$$

$$\tilde{z}_{(\xi,\eta)} = \bar{r}\sin\left\{\bar{\theta} + \frac{c}{r}\left[(\xi - \bar{\xi})\sin\beta - \tilde{\zeta}\cos\beta\right]\right\} \tag{116}$$

These equations can be used to construct the cartesian coordinates for any other set of $\zeta(\xi; \eta)$ curves, such as the upper and lower blade surfaces.

14.3 Normal-vector construction

For constructing a flow-tangency condition on the blade surface, it is typically necessary to define a vector $\hat{n}$ normal to the camber surface at some chosen chordwise location ξ_n. For the vortex lattice

18

method, this would be at the $\xi_n = 3/4$ position. We first define cartesian vectors $\vec{u}_\xi$ and $\vec{u}_\eta$ which lie on the camber surface at the chosen ξ_n location, and point in the ξ and η directions.

$$\vec{u}_{\xi(\eta)} = \left[\frac{\partial \tilde{x}}{\partial \xi}\hat{i} + \frac{\partial \tilde{y}}{\partial \xi}\hat{j} + \frac{\partial \tilde{z}}{\partial \xi}\hat{k} \right]_{\xi=\xi_n} \tag{117}$$

$$\vec{u}_{\eta(\eta)} = \left[\frac{\partial \tilde{x}}{\partial \eta}\hat{i} + \frac{\partial \tilde{y}}{\partial \eta}\hat{j} + \frac{\partial \tilde{z}}{\partial \eta}\hat{k} \right]_{\xi=\xi_n} \tag{118}$$

The cartesian normal unit vector is then readily computed via a cross product and normalization.

$$\vec{n}_{(\eta)} = \vec{u}_\xi \times \vec{u}_\eta \tag{119}$$

$$\hat{n}_{(\eta)} = \frac{\vec{n}}{|\vec{n}|} \tag{120}$$

15 Overall Solution Strategy

The solution procedure for a typical rotor analysis problem is described below.

15.1 Inputs

Rotor blade geometry:	$c(r)$, $\beta(r)$
Rotor aero properties:	$\alpha_o(r)$, $m_{2D}(r)$, $c_d(r)$
Duct and hub geometry:	$x(s)$, $r(s)$
Drag object properties:	r, z, A_D
Freestream speed:	V_∞
Rotor rotational speed:	Ω

15.2 Initial Grid via Zero-thrust, Unit-V_∞ solution

1. Define paneling on duct and hub

2. Evaluate for panel control points: $\hat{n}_i$, $\bar{a}_{x_{ij}}$, $\bar{a}_{r_{ij}}$

3. Assemble $\bar{a}_{ij}$, augment with Kutta condition

4. LU-Factor $\bar{a}_{ij}$ $\rightarrow$ $\bar{a}_{ij}^{-1}$

5. Back-substitute for $\bar{\gamma}_{o_i}$

6. Set initial streamfunction grid, assign grid ξ values

7. Evaluate $v_{x\,o_i}$, $v_{r\,o_i}$ at grid boundaries

8. Use $v_{x\,o_i}$, $v_{r\,o_i}$ to compute ψ and assign grid η

9. Set $Q_1 = 0$

10. Relax grid with SLOR, using $v_{x\,o_i}$, $v_{r\,o_i}$ for Neumann boundary conditions

15.3 Rotor-On Solution

Iteration setup:

1. Define paneling on grid streamsurfaces, define source drag panels

2. Evaluate at body panels, rotor blade stations, source drag panels: $a_{x_{ij}}, a_{r_{ij}}, a_{ij}, b_{x_{ij}}, b_{r_{ij}}, b_{ij}$

3. Set initial guess for Γ_k

4. Set corresponding $\tilde{\Gamma}$ and $\tilde{H}$ fields

5. Set initial guess for γ_i using (41) and (42)

6. Set initial $\sigma_i = 0$

One Newton iteration:

1. Using current Γ_k, σ_i, evaluate γ_i, v_{x_i}, v_{r_i}, v_{θ_i}, $\vec{V}_i$ and derivatives w.r.t. Γ_k, σ_i

2. Evaluate residuals of equations (75), (73), (74), and derivatives w.r.t. Γ_k, σ_i

3. Solve Newton system for $\delta\Gamma_k$, $\delta\sigma_i$

4. Update Γ_k, σ_i

Streamline grid update (after Newton convergence)

1. Evaluate $\vec{V}$ at grid cells, using grid derivatives

2. Evaluate $\tilde{\Gamma}$, $\tilde{H}$, $\tilde{S}$ for all grid cells downstream of blade stations and drag-producing objects (source panels)

3. Evaluate Q_1 for all grid cells

4. Relax grid via SLOR

5. Begin again at "Iteration setup"

References

[1] A. Betz. Airscrews with minimum energy loss. Report, Kaiser Wilhelm Institute for Flow Research, 1919.

[2] H. Glauert. *Elements of Airfoil and Airscrew Theory*. Cambridge University Press, Cambridge, 1937.

[3] J.F. Thompson, F.C. Thames, and C.W. Mastin. Automatic numerical generation of body-fitted curvilinear coordinate system for field containing any number of arbitrary two-dimensional bodies. *Journal of Computational Physics*, 15:299–319, 1974.